Neurobiology of Disease 121 (2019) 274–285

Contents lists available at ScienceDirect

Neurobiology of Disease

journal homepage: www.elsevier.com/locate/ynbdi

PRRT2 deficiency induces paroxysmal kinesigenic dyskinesia by influencing synaptic function in the primary motor cortex of rats

Juan Mo[1], Bantong Wang[1], Xilin Zhu, Xiaopan Wu, Ying Liu*

State Key Laboratory of Medical Molecular Biology, Institute of Basic Medical Sciences, Chinese Academy of Medical Sciences, School of Basic Medicine, Peking Union Medical College, Beijing 100005, China

ARTICLE INFO

Keywords:
PRRT2
Paroxysmal kinesigenic choreoathetosis
M1 cortex
SNARE complex
Synaptic transmission

ABSTRACT

Proline-rich transmembrane protein 2 (*PRRT2*) was identified as the causative gene of paroxysmal kinesigenic choreoathetosis (PKC) as well as various other neurological diseases. However, the molecular mechanisms of how mutant PRRT2 leads to abnormal synaptic function and triggers PKC are still obscure. We generated a *Prrt2* truncated mutant rat model which shows spontaneous PKC-like attacks with a relative low frequency as well as increased susceptibility to pentylenetetrazol (PTZ)-induced seizures. We demonstrate that PRRT2 is expressed on both pre- and post-synaptic membranes in the M1 cortex. PRRT2 negatively regulates SNARE complex assembly through interaction with SNAP25, STX1A, and VAMP2. In the M1 cortex of the rat model, release of amino acid neurotransmitters is increased. Protein levels of glutamate receptor subunit GRIA1 are significantly increased in PRRT2 mutant rats, while GABA receptor subunits GABRA1 are significantly reduced. Both frequency and amplitude of mEPSC are significantly increased, while amplitude of mIPSC is decreased and the ratio of mEPSC/mIPSC is significantly increased. The balance between excitatory and inhibitory neuronal activity is disrupted, which could lead to abnormal neuronal hyperexcitability. These results provide new insights into the function of PRRT2 in synaptic transmission and movement control, as well as the pathogenic mechanism underlying PKC.

1. Introduction

Paroxysmal kinesigenic choreoathetosis (PKC, OMIM 128200), first reported by Kertesz in 1967 (Kertesz, 1967) and characterized by recurrent and brief attacks, is the most common hereditary paroxysmal movement disorder (Bhatia, 2011; Ebrahimi-Fakhari et al., 2015). The attacks are usually triggered by sudden voluntary movements. Symptoms during the ictal period typically include unilateral or bilateral involuntary movements, such as chorea, athetosis, dystonia, etc. (Goodenough et al., 1978; Demirkiran and Jankovic, 1995; Klein and Vieregge, 1998; Bruno et al., 2004).

It has been reported that the occurrence of PKC was associated with the motor circuits (i.e., cortical-basal ganglia-thalamo loops and cortical-cerebellar system) (Ren et al., 2015; Long et al., 2017; Michetti et al., 2017) and abnormal neuronal hyperactivity in the cortex and basal nuclei or in the thalamus was responsible for the pathophysiology of PKC (Shirane et al., 2001; Zhou et al., 2010). However, Fattapposta F et al. reported that the PKC patient presented a disorder of temporal organization of a voluntary motor response to a stimulus. Both a clinical improvement and normalization of motor-related electrophysiological anomalies were observed during therapy (Fattapposta et al., 2003). The research using resting-state functional magnetic resonance imaging (rfMRI) showed that the most pronounce functional change was located in the anterior areas of the motor circuit, which were related to motor preparation and initiation (Luo et al., 2013). There were also other previous researches suggested that PKC was a disorder concerning motor and premotor cortex (Franssen et al., 1983; Busard et al., 1984). So, it is obvious that the motor cortex is very important for the pathogenesis of PKC. Nonetheless, the exact pathogenesis of PKC is still unknown. A PKC locus was mapped to 16p11.2-q12.1 (Ha et al., 1999). Our previous study verified this conclusion (Du et al., 2008; Wang et al., 2010) and we also described the gene mutation spectrum of PKC (Li et al., 2012). Meanwhile, many studies have confirmed that mutations in proline-rich transmembrane protein 2 (*PRRT2*) are associated with various neurological diseases, including paroxysmal kinesigenic dyskinesia (PKC) (Chen et al., 2011; Wang et al., 2011; Cao et al., 2012), benign familial infantile epilepsy (BFIE, OMIM 605751) (Schmidt et al., 2012; Schubert et al., 2012; Okumura et al., 2013), infantile convulsions and choreoathetosis (ICCA, OMIM 602066) (Heron et al., 2012; Lee et al., 2012), and others (Liu et al., 2012; Ono

* Corresponding author.
E-mail address: liuyingpumc@163.com (Y. Liu).
[1] Juan Mo and Bantong Wang contributed equally to this work.

https://doi.org/10.1016/j.nbd.2018.10.011
Received 5 October 2018; Received in revised form 16 October 2018; Accepted 17 October 2018
Available online 19 October 2018
0969-9961/

et al., 2012; Marini et al., 2012), which are all termed as "*PRRT2*-related disorders" (Becker et al., 2013; Méneret et al., 2013).

Studies on mice revealed that *Prrt2* is specifically expressed in neural tissues with especially high levels in the cerebral cortex, hippocampus, and cerebellum (Lee et al., 2012; Chen et al., 2011; Heron et al., 2012). PRRT2 contains 340 amino acids (Lee et al., 2012) with an extracellular hydrophobic C-segment spanning the plasma membrane and an intracellular proline-rich hydrophobic N-segment forming a helix-loop-helix structure without crossing the plasma membrane (Rossi et al., 2016).

Stelzl et al. found that PRRT2 interacts with the synaptosomal-associated protein SNAP-25 (Stelzl et al., 2005), which is a key element of the SNARE (soluble N-ethylmaleimide-sensitive factor attachment protein receptor) complex and critical for exocytosis of neurotransmitters (Yang et al., 2000). Meanwhile, it was found that the interaction between mutant PRRT2 and SNAP25 is significantly decreased (Lee et al., 2012; Li et al., 2015). A high-resolution proteomics analysis offered an additional important clue for the function of PRRT2, identifying that PRRT2 is associated with GRIA1, a subunit of native α-amino-3-hydroxy-5-methyl-4-isoxazolepropionic acid (AMPA) receptor complexes, which are one of the ionotropic glutamate receptors (Schwenk et al., 2012). Further studies showed that PRRT2 could also interact with synaptotagmin, which is an important calcium sensor for evoked vesicle release (Valente et al., 2016). Recently, Tan et al. found that PRRT2 can regulate formation of the SNARE complex, and that conditional knockout of *Prrt2* in cerebellar granule cells (GCs) is sufficient to induce dyskinesic attacks (Tan et al., 2018).

Together, all of the reports described above suggest that PRRT2 may participate in the release of neurotransmitters and influence the function of synapses. In addition to the synaptic functions, Fruscione F et al. reported an extrasynaptic role of PRRT2 that it is an important negative modulator of Nav1.2 and Nav1.6 channels. (Fruscione et al., 2018). However, the molecular mechanisms by which mutant PRRT2 leads to abnormal synaptic function and causes the symptoms that define PKC are still obscure.

In this study, we investigated the interactions between PRRT2 and synaptic proteins, the fusion and release of vesicles, concentrations of amino acid neurotransmitters, protein levels of receptors, and electrophysiologic parameters of primary motor cortex (M1) neurons of a CRISPR/Cas9-generated *Prrt2* truncated mutant rat. The primary motor cortex (M1), a central part of the motor circuit of basal ganglia-thalamo-cortical loops, is the core motor cortex, and is closely related to motor behaviors. Our study elucidated that expression of a PRRT2 truncated mutant in this region could cause abnormal synaptic function by increasing neurotransmitter release, leading to neuronal hyperexcitability and ultimately seizures characteristic of PKC. Further elucidating the underlying pathologic molecular mechanisms could provide potential therapeutic targets for individuals with PKC.

2. Materials and methods

2.1. Animals

All Sprague Dawley (SD) rats used in the experiments were 4–6 week-old littermates of the same sex. The generation of *Prrt2*^{mut} rats was entrusted to Laboratory Animal Sciences, Chinese Academy of Medical Sciences, Peking Union Medical College (CAMS & PUMC). Briefly, a truncated mutant rat model with 460 bp deleted from the second exon (nucleotides 80th–539th) of *Prrt2* was generated using CRISPR/Cas9-mediated gene editing technology. As a result, translation of the mutant *Prrt2* was prematurely terminated, which resembles the *Prrt2* mutation in PKC patients. Genotypes and sex of every neonatal rat were identified by PCR and agarose gel electrophoresis. Rats were raised in the Institute of Laboratory Animal Sciences, CAMS & PUMC. Ambient housing conditions were 22 ± 1 °C with 56%–60% humidity. Animals were caged with food and water available ad libitum with 12 h light-dark cycle. Animal husbandry and experimental protocols were approved by the Institutional Animal Care and Use Committee at the Institute of Basic Medical Sciences, Chinese Academy of Medical Sciences and Peking Union Medical College and complied with Experimental Animal Regulations.

2.2. Immunostaining

Brains were dissected immediately after decollation and soaked in 4% paraformaldehyde (PFA) for 48 h. Paraffin-embedded tissues were cut into 4 μm thick sections and laid on slides. Slides were dewaxed in dimethylbenzene and rehydrated in gradient concentrations of alcohol, then incubated with methanol-perhydrol solution for 10 min at room temperature. Antigen retrieval was carried out with citrate buffer through microwave radiation. Slides were blocked with goat serum for 20 min at room temperature and then incubated in a humidifying box with the primary antibodies (rabbit anti-PRRT2, Sigma, HPA014447, 1:200; mouse anti-PRRT2, Abcam, ab219960, 1:50; rabbit anti-NeuN, Proteintech, 26,975–1-AP, 1:100; rabbit anti-GFAP, Proteintech, 16,825–1-AP, 1:100; rabbit anti-GAD65 + GAD67, Abcam, ab183999, 1:100; rabbit anti-vGLUT1, Proteintech, 55,491–1-AP, 1:10; rabbit anti-SYP, Proteintech, 17,785–1-AP, 1:10; rabbit anti-PSD95, Proteintech, 20,665–1-AP, 1:10) at 4 °C overnight. The following day, sections were rinsed with PBS. For immunofluorescence, slides were incubated with fluorescence-labeled corresponding secondary antibodies (goat anti-mouse IgG, FITC conjugated, CWBIO, CW0113, 1:100; goat anti-rabbit IgG, TRITC conjugated, CWBIO, CW0160, 1:100) which were then rinsed with PBS for 30 min at room temperature. Sections were mounted with mounting medium containing DAPI (ZSGB-BIO, ZLI-9557) and observed by confocal microscopy (LSM 780, Zeiss). For immunohistochemistry, slides were incubated with biotin-labeled corresponding secondary antibodies, rinsed with PBS for 30 min at room temperature, and then incubated with horseradish-peroxidase conjugated streptavidin for 30 min at room temperature (Histostain™-SP Kits, ZSGB-BIO, SPN-9002). Slides were stained with DAB, and washed with water to stop the reaction. Counterstaining was performed with hematoxylin. Slides were dehydrated in gradient concentrations of alcohol, cleared in dimethylbenzene, then mounted.

2.3. Western Blot

Tissues were removed, weighed, and homogenized in RIPA buffer (w/v = 1:10) (RIPA Lysis Buffer [Medium], CWBIO, CW2334) then centrifuged at 12,000g for 15 min at 4 °C. Supernatant protein concentration was quantified by BCA assay (BCA Protein Assay Kit, CWBIO, CW0014). The supernatant solution was added with loading buffer and heated to 95 °C for 15 min. Protein samples (35 μg/lane) were separated by SDS-PAGE and transferred to nitrocellulose membranes which were then blocked with 5% nonfat milk in TBST (Tris-buffered saline containing 0.1% Tween-20) for 1 h at room temperature. The membranes were then incubated with primary antibodies (rabbit anti-PRRT2, Sigma, HPA014447, 1:1000; rabbit anti-VAMP2, Abcam, ab181869, 1:10000; rabbit anti-SNAP25, Abcam, ab5666, 1:10000; rabbit anti-Syntaxin 1a, Abcam, ab41453, 1:1000; rabbit anti-Synaptotagmin 1, Abcam, ab82414, 1:1000; rabbit anti-GRIA1, Abcam, ab109450, 1:1000; rabbit anti-GABRA1, Proteintech, 12,410–1-AP, 1:1000; mouse anti-β-actin, CWBIO, CW0096M,1:5000; rabbit anti-GAPDH, CWBIO, CW0101M, 1:5000) at 4 °C overnight. Membranes were washed with TBST, then incubated with corresponding secondary antibodies (Goat Anti-Rabbit IgG, HRP Conjugated, CWBIO, CW0103, 1:10000; Goat Anti-Mouse IgG, HRP Conjugated, CWBIO, CW0102, 1:10000) for 2 h at room temperature. cECL Western Blot kit (CWBIO, CW0048) was used to detect the blots. The optical densities of proteins were determined by Image J 1.48 software.

2.4. Isolation of PSDs

The procedure used to isolate PSDs from rat brain was a modification of the procedure used by Cohen RS et al. (Cohen et al., 1977). The brain was removed from a rat, dissected into four parts, then rinsed in solution A (0.32 M Sucrose, 1 mM $NaHCO_3$, 1 mM $MgCl_2$, 0.5 mM $CaCl_2$). Homogenization was performed with an electrically-driven tissue homogenizer (T10 Basic, IKA), using 10 g brain tissues/40 mL of solution A. The resulting homogenates were combined and diluted to 10% (*w/v*) in solution A. A low speed (1400 g) pellet was obtained and washed by resuspending the pellet in the same 10% volume of solution A. The second centrifugation (710*g*) was carried out for 10 min. After centrifugation, the precipitate (P1) was discarded, and the supernatants (S1) were pooled and centrifuged at 13,800 *g* for 10 min. The supernatant (S2) was discarded. The resulting pellet (P2), containing synaptosomes and mitochondria, was resuspended in solution B (0.32 M Sucrose, 1 mM $NaHCO_3$) using 24 mL/10 g starting tissue. Sucrose gradient centrifugation was performed using a SW 27 rotor (Beckman Instruments, Inc.) with 8 mL of the resuspended material and 10 mL each of 0.85, 1.0, and 1.2 M sucrose solutions all containing 1.0 mM $NaHCO_3$. These gradients were then run for 2 h at 82500*g*. The band between 1.0 and 1.2 M sucrose contained synaptosomes (Syn). Synaptosomes were diluted with solution B (60 mL/10 g initial weight), an equal volume of 1% (*v*/v) Triton X-100 in 0.32 M sucrose, 12 mM Tris-HCl (pH 8.1) was added, and the resulting, somewhat clarified suspension was stirred in the cold for 15 min. This suspension was centrifuged at 32,800*g* for 20 min, and the pellet was resuspended in 2.5 mL of solution B/ 10 g original wet weight brain. 2 mL of this material was layered in polyallomer tubes on gradients composed of 4 mL of 2.0 M sucrose, 3.0 mL of 1.5 M sucrose, 1 mM $NaHCO_3$, and 3.0 mL of 1.0 M sucrose, 1 mM $NaHCO_3$. The gradients were centrifuged for 2 h at 201,800*g* in a SW 40 rotor (Beckman Instruments, Inc.). The PSD-containing band between 1.5 and 2.0 M sucrose was collected and diluted to a final volume of 6.0 mL with solution B, and an equal volume of 1% Triton-100, 150 mM KCl was added. This suspension was centrifuged for 20 min at 20,180*g* in a SW 40 rotor. The resulting pellet was purified PSDs.

2.5. Co-immunoprecipitation

Total protein extraction (Native lysis buffer, Solarbio, R0030) and quantification was performed as described earlier. 500 μg total protein was added with 2 μg primary antibodies (mouse anti-PRRT2, Abcam, ab219960; mouse anti-SNAP25, Abcam, ab66066; mouse anti-VAMP2, Santa Cruz, sc-69,706) or IgG (normal mouse IgG, Santa Cruz, sc-2025) at 4 °C overnight. Then 30 μL protein A/G plus-Agarose (Santa Cruz, sc-2003) was added to the lysate. The mixtures were incubated for 3 h, then centrifuged at 2500*g* for 5 min at 4 °C. The precipitates were rinsed with PBS and centrifuged at 2500*g* for 5 min at 4 °C three times. Finally, the precipitates were resuspended in 30 μL loading buffer and denatured at 95 °C for 15 min.

2.6. Microdialysis

The recovery capacity of microdialysis probes (CMA/Microdialysis) was determined using a mixture of standards prior to experiments. After rats were weighed and anesthetized, a microdialysis probe sleeve (MAB2/6/9, Microbiotech) was implanted into the given coordinates in the M1 cortex. According to *The Rat Brain in Stereotaxic Coordinates* (Paxinos and Watson, 2007) the coordinates, with the bregma as the origin, were 3.2 mm in front bregma, 2.8 mm right of the median suture, and 1.2 mm depth. The probe was inserted every other day. The rats were perfused with sodium chloride injection at a flow rate of 1 μL/min. Samples were collected after one hour equilibration.

2.7. High performance liquid chromatography

The concentrations of aspartate, glutamate, glycine, and GABA were analyzed by high performance liquid chromatography (HPLC) (Sykam, Germany) with a fluorescence detector (Shimadzu, Japan). Agilent Eclipse AAA column (5 μm, 4.6 × 150 mm) was used with mobile phase A (20 mM sodium acetate solution: methanol:tetrahydrofuran = 400:95:5) and mobile phase B (20 mM sodium acetate solution:methanol = 120:380). The gradient elution procedure of mobile phase B was: 0–10 min: 0%–63%, 10–12 min: 63%, 12–17 min: 100%, 17–18 min: 100%–0%, 18–21 min: 0%. The flow rate was 0.8 mL/min. The excitation wavelength was 340 nm. The emission wavelength was 455 nm. A mixed amino acids solution of 200 ng/mL, 100 ng/mL, 50 ng/mL, 25 ng/mL, 12.5 ng/mL were used as standard. In preparation for detection, tissues were weighed and homogenized in a solution of ddH_2O and acetonitrile (ddH_2O: acetonitrile = 2:3). They were then further disintegrated by ultrasound for 20 min and centrifuged at 15,000 rpm for 10 min at 4 °C. The supernatant was further centrifuged at 15,000 rpm for 5 min at 4 °C, and the resulting supernatant was used for detection. Microdialysis samples were used directly for detection. All samples were derivatized with O-phthaldialdehyde (OPA) prior to detection.

2.8. Transmission electron microscopy

5-week-old rats were transcardially perfused with 2.5% glutaraldehyde (Sigma, G6257) for 20 min. Brains were then immersed in fixative solution containing 2% paraformaldehyde (PFA) and 2.5% glutaraldehyde for 2 h at 4 °C. Cortex blocks were washed in PBS (pH 7.2) and treated with 1% osmium tetroxide in PB for 2 h, then dehydrated in a series of ethanol and flat embedded in epoxy resin (EPON 812 Polysciences). After polymerization, blocks from the M1 cortex were cut at 60–80 nm and stained with uranyl acetate-lead citrate. Using a digital camera attached to a Hitachi 7650 electron microscope operated at 80 kV, at least 10 images of synapses were acquired at 25,000 magnification. Number of synaptic vesicles and "docked" vesicles at the active zone were determined using ImageJ software.

2.9. Electrophysiology

Rats were deeply anesthetized with ether and decapitated. The brain was rapidly removed from the skull with the least amount of damage and pressure onto the brain. The brain was then transferred into ice-cold artificial cerebrospinal fluid (ACSF, mM: 124 NaCl, 2.5 KCl, 1.2 NaH_2PO_4, 24 $NaHCO_3$, 12.5 D-Glucose, 2 $CaCl_2$, and 1.5 $MgSO_4$ saturated with 95% O_2 and 5% CO_2, pH 7.3). A filter paper was placed on the bottom of one petri dish in advance. Using a spoon, the brain was transferred into the petri dish containing ice-cold ACSF and placed with the ventral side of the brain touching the filter paper. 300 μm-thick slices were cut with a Vibratome (Leica, VT 1000 S, Germany), which was filled with cold ACSF. The prepared slices were incubated in oxygenated ACSF at room temperature for at least 1 h, and then individual slices were transferred to a recording chamber, which was bubbled with oxygenated ACSF at 31 ± 1 °C and the perfusion rate adjusted to 2 mL/min. Electrophysiological recordings were obtained under visual control by use of an Olympus microscope (Olympus BX50-WI, Olympus, Japan) and a 40× long-working distance objective (NA 0.8). Patch pipettes with 4–6 MΩ resistance were pulled from 110 mm long borosilicate glass capillaries (GB 150F−8P, Sutter instruments, USA). Ion currents were recorded using an Axopatch 700B amplifier and pClamp10.6. Recordings of spontaneous miniature postsynaptic miniature currents were done in whole cell mode. The signal was obtained at a holding potential of −80 mV. For pharmacological isolation of AMPA receptor-mediated mEPSCs, 1 μM TTX and 100 μM PTX were added to the ACSF. The intracellular solution used was (in mM): 140 K-

gluconate, 2 $MgCl_2$, 8 KCl, 10 HEPES, 0.2 NaGTP, 2 Na_2ATP. The pH was adjusted to 7.3 with KOH. The extracellular solution contained TTX (1 μM) for recording mEPSCs. For each cell, at least 5 min of recording was obtained. For the detection of spontaneous events, the "threshold research" option was used and each event was checked. To record mIPSCs, 1 μM TTX and 20 μM DNQX were added into the ACSF. The signal was obtained at a holding potential of −80 mV. The intracellular solution used was (in mM): 140 CsCl, 2 $CaCl_2$, 2 $MgCl_2$, 1.1 EGTA, 2 Na_2-ATP, 10 HEPES. The pH was adjusted to 7.3 with CsOH. The glass stimulation electrode was placed at Layer II/III at a distance of 100–200 μm from the recording cell, and the time of stimulation was 0.05 ms. The holding potential of AMPA recording was -55 mV. For measuring GABA-mediated currents, the holding potential was +30 mV and 50 μM D-AP5 was added to ACSF. The intracellular solution used was (in mM): 135 Cs-methanesulfonate, 2 $MgCl_2$, 10 NaCl, 10 HEPES, 0.2 NaGTP, 2 Na_2ATP, 10 EGTA, 5 QX-314. The pH was adjusted to 7.3 with CsOH.

2.10. Somatic growth and spontaneous movements in rat pups

Rats of three genotypes at the ages of postnatal day 4, 8, 12, and 16 were measured for body weight, body length, tail length, and axillary temperature. Rats were then monitored for 1 h by video recording for spontaneous PKC-like attacks.

2.11. PTZ-induced seizures

Wild type and knockout littermates were injected with the same dose of PTZ (Sigma, P6500) (60 mg/kg intraperitoneally in 0.9% saline) and continuously monitored in a 35 × 25 × 25 cm box until they returned to baseline.

2.12. Balance beam

The beam apparatus consisted of 1 m beams with a flat surface of 10 mm width resting 50 cm above the ground. A dark home cage was placed to attract the rat to the finish point. A lamp was used to shine light above the start point and served as an aversive stimulus. The time to cross the beam and the number of slippages was recorded.

2.13. Coat-hanger test

A 40 cm length x 3 mm diameter coat hanger-like apparatus was made to assess muscle strength and motor coordination. The apparatus was placed at a 40 cm distance from the ground and the rats were placed onto it with their forelimbs grasping the center on a horizontal axis. The test lasts for 30 s. The performance scores were rated as follows: 0-fall within 10 s; 1- forelimbs hanging on the coat hanger; 2-attempt to climb onto the coat hanger; 3- forelimbs and at least one hindlimb hanging on the coat hanger; 4-all four limbs and tail twining around the horizontal axis; 5-attempt to escape to the end of the horizontal axis.

2.14. Grip strength test

5-week-old wild type and mutant rats were individually placed on the grip strength apparatus (Bioseb); the tail was then gently pulled and grip strength recorded. Each rat was tested three times with the average reported.

2.15. Open field test

To measure locomotor activity and anxiety-like behavior, rats were individually placed in an opaque open field test (50 × 50 × 50 cm). The session started by placing the animal in the center followed by 5 min of observation. The mean speed, total distance, and time spent in the center and in the border were recorded automatically.

2.16. Fear conditioning test

The Video Tracking of Fear Conditioning System (MED Associates) was used to assess the ability of rats to learn to predict aversive events. In brief, rats were placed into a conditioning chamber and given parings of conditioned stimulus (an auditory cue) and an aversive unconditioned stimulus (an electric foot shock) on the first day. At the same time on the second day, rats were exposed to the same conditioning chamber without any stimulus, and the freezing time in 5 min was recorded. After 24 h, rats were placed into a chamber with a change of background environment and smell, with 3 min allowed for adaptation. After this interval, the same pairings of auditory stimuli as given on the first day were given, and the freezing time over 5 min was recorded.

2.17. Acoustic startle response and PPI

Prepulse inhibition of startle (PPI) was measured by the startle reflex apparatus (MED Associates). There were three blocks: block 1 containing 10 startle stimuli (120 dB) which lasted 40 ms; block 2 containing 10 startle stimuli, 10 NOSTIM, 30 prepulse stimulus inhibition test. Three different prepulse intensities were used (70 dB, 75 dB, and 80 dB), and the intervals of the prepulse and startle stimulus was 100 ms. Inter-trial intervals were randomized between 27 and 32 s.

2.18. Statistical analysis

All experiments and data analysis were performed by investigators masked to the rat genotypes and treatments. Data were presented as mean ± SEM. Comparison between two groups was analyzed by Student's *t*-tests. $P < .05$ was considered statistically significant.

3. Results

3.1. The expression and location of PRRT2

PRRT2 was expressed specifically in the nervous system but scarcely in other organs (Fig. 1A). The expression levels increased sharply after birth, and remained stable in rats up to 4–6 weeks old (Fig. 1B). PRRT2 was specifically expressed in neurons but was absent from neuroglia cells (Fig. 1C). It existed in both glutamatergic neurons and GABAergic neurons (Fig. 1D). Results of IF staining and Western Blot of isolated postsynaptic densities (PSDs) indicated that PRRT2 was expressed on both pre- and post-synaptic membranes (Fig. 1E and F), suggesting its potential role in regulating synaptic transmission.

3.2. Corroborating the $Prrt2^{mut}$ rat model

Most *PRRT2* mutations in clinical patients are located within the second exon. These PRRT2 variants lead to truncated proteins, consistent with loss-of-function and haploinsufficiency (Li J et al., 2011; Liu et al., 2016; Valtorta et al., 2016). The mutant *Prrt2* in our rat model resembles it in PKC patients (Fig. 2A-C). No PRRT2 expression was detected in the $Prrt2^{-/-}$ rat (Fig. 2D). Meanwhile, PRRT2 levels in the $Prrt2^{+/-}$ rats were approximately half that of wild type, demonstrating haploinsufficiency (Fig. 2E). Immunohistochemical (IHC) staining results were consistent with the Western analysis (Fig. 2F), corroborating that the *Prrt2* gene was successfully knocked out.

3.3. Phenotypic assessment of $Prrt2^{mut}$ rat model

Since PRRT2 expression showed a rapid rise in the nervous system of postnatal day 3 rats and PKC symptom onset in humans occurs primarily during adolescence, we examined the weight, body length, tail length, and body temperature of $Prrt2^{+/+}$, $Prrt2^{+/-}$, and $Prrt2^{-/-}$ rats

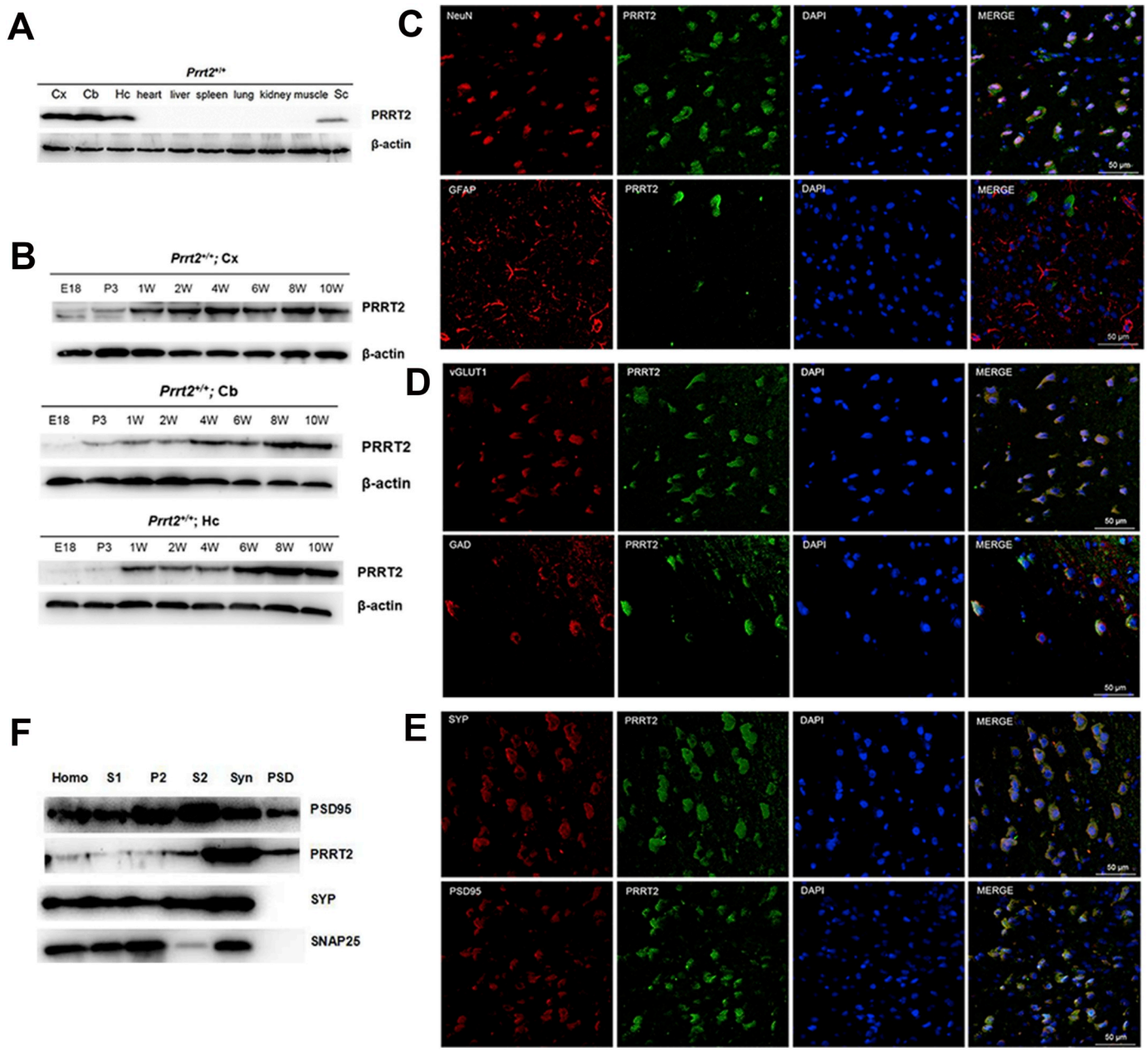

Fig. 1. Expression pattern and subcellular localization of PRRT2.

(A) Western blot detected the specific expression of PRRT2 in the nervous system with scarce or absent expression in other tissues. β-actin served as an internal control. (Cx, cerebral cortex; Cb, cerebellum; Hc, hippocampus; Sc, spinal cord)
(B) Western blot results confirmed that PRRT2 expression had a sharp increase after birth in the cerebral cortex, cerebellum, and hippocampus, and remained stable in rats up to 4–6 weeks old. β-actin served as an internal control.
(C) IF staining suggested that PRRT2 was specifically expressed in neurons with no expression detected in neuroglia cells in M1. Scale bar, 50 μm.
(D) IF staining showed that PRRT2 was present in both glutamatergic neurons and GABAergic neurons in M1. Scale bar, 50 μm.
(E) IF staining verified that PRRT2 was expressed in both pre- and post-synaptic membranes in M1. Scale bar, 50 μm.
(F) PRRT2 and PSD95 were present and co-fractionated in postsynaptic compartments. SYP and SNAP25 were not present in postsynaptic compartments. Homo = homogenate, S1 = low-speed supernatant, P2 = synaptosomes and mitochondria, S2 = microsomes and ribosomes, Syn = synaptosomes (including pre- and post-synaptic membrane), PSD = postsynaptic densities.

at postnatal days 4, 8, 12, and 16. There was no significant difference for these parameters among the three genotypes (Fig. 3A). At the same time, we monitored and recorded behaving *Prrt2*$^{+/+}$ and *Prrt2*$^{-/-}$ rats and observed spontaneous PKC-like attacks in *Prrt2*$^{-/-}$ rats with a relatively low frequency (Fig. 3B and Supplementary Information Video 1 and Video 2).

Furthermore, we conducted a series of behavioral tests to validate the PKC rat model. As shown, *Prrt2*$^{-/-}$ rats not only required more time to pass through the same beam (+/+, 4.54 ± 0.26 s; −/−, 7.81 ± 0.37 s, $P < .0001$) (Fig. 3C), but also had lower scores in the coat hanger test (+/+, 4.33 ± 0.29; −/−, 1.67 ± 0.47, $P = .0039$) (Fig. 3D).

In addition, following intraperitoneal injection (i.p.) of the same dose of pentylenetetrazol (PTZ, 60 mg/kg), *Prrt2*$^{-/-}$ rats showed a significantly higher seizure frequency (+/+, 6/12; −/−, 11/12) and longer duration of 5-rated seizures compared to wild type littermates

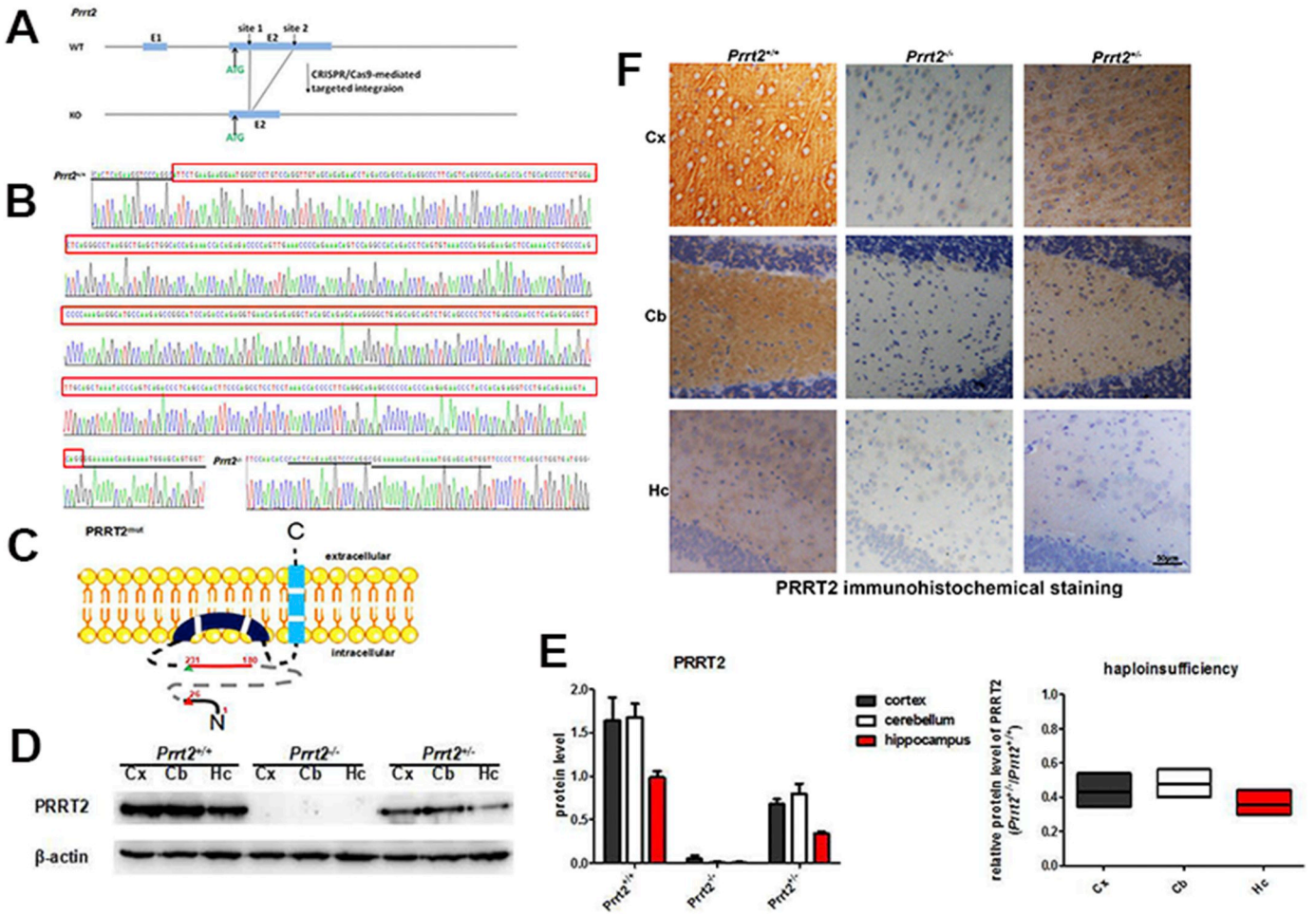

Fig. 2. Generation of *Prrt2*^{mut} rat model by CRISPR/Cas9-mediated gene editing technology.

(A) Diagram of 460 bp deletion from the second exon (nucleotides 80–539) of *Prrt2* on SD rat background.
(B) DNA sequencing demonstrated that 460 nucleotides (shown in red box) had been deleted in *Prrt2*$^{-/-}$ rat compared to *Prrt2*$^{+/+}$ rat.
(C) Schematic representation of PRRT2 truncated mutant in our rat model with a membrane topology of PRRT2 as reported by Rossi et al. (Rossi P, et al. 2016). black solid line, normal translated residues; red triangle, initial mutation site; gray dotted line, deleted residues; red solid line, frameshift mutation residues; green triangle, translation termination.
(D-E) Western blot showed absence of PRRT2 in the cerebral cortex, cerebellum, and hippocampus of *Prrt2*$^{-/-}$ rats, with the PRRT2 level of the *Prrt2*$^{+/-}$ rat consistent with haploinsufficiency. (D) Representative immunoblots. β-actin served as an internal control. (E) Quantification of Western blot results. Error bars, mean ± SEM; $n = 3$.
(F) Representative IHC staining of PRRT2 in the cerebral cortex, cerebellum, and hippocampus of 35 day-old *Prrt2*$^{+/+}$, *Prrt2*$^{+/-}$, and *Prrt2*$^{-/-}$ rats. Scale bar, 50 μm.

(+/+, 41.40 ± 9.41 s; −/−, 85.11 ± 13.10 s, $P = .0414$) (Fig. 3E). The seizure rate was defined as Racine described in 1972 (Racine, 1972). However, other behaviors of *Prrt2*$^{-/-}$ rats were normal, including open field test, fear conditioning, acoustic startle response, and prepulse inhibition of startle (PPI) (Supplementary Information, Fig. S1), which agreed with clinical observations.

3.4. PRRT2 inhibits assembly of the SNARE complex

PRRT2 is likely involved in the fusion of synaptic vesicles with the pre-synaptic membrane, followed by release of neurotransmitters (Li et al., 2015; Valente et al., 2016; Valtorta et al., 2016). The assembly of the SNARE complex is a critical featured required for vesicular fusion (Jahn and Fasshauer, 2012; Coleman et al., 2018; Tan et al., 2018). Compared to *Prrt2*$^{+/+}$ rats, protein levels of the SNARE elements all rose significantly in the M1 cortex of *Prrt2*$^{-/-}$ rats, but not in cerebellar or hippocampal tissues of *Prrt2*$^{-/-}$ or *Prrt2*$^{+/-}$ rats. The level of SYT1 has the same trend in *Prrt2*$^{-/-}$ rats (Fig. 4A and B). Therefore, we hypothesized that mutation of PRRT2 in the M1 cortex had a close association with the clinical symptoms, and as described later, defined how PRRT2 plays a role in synaptic transmission in this region.

Co-immunoprecipitation (co-IP) results indicated that PRRT2 interacted with SNAP25, syntaxin 1A (STX1A), and VAMP2, but not with SYT1 in the M1 cortex of *Prrt2*$^{+/+}$ rats (Fig. 4C); these findings differ from studies in mice (Valente et al., 2016). To verify assembly of the SNARE complex, we also detected the interaction between SNAP25 and VAMP2 by co-IP. Compared to *Prrt2*$^{+/+}$ rats, the interaction between SNAP25 and VAMP2 was significantly higher in the M1 cortex of *Prrt2*$^{-/-}$ rats (Fig. 4D and E). This result indicated that assembly of the SNARE complex is increased in the absence of functional PRRT2, suggesting that PRRT2 negatively regulates SNARE complex assembly.

3.5. PRRT2 deficiency is associated with increased release of amino acid neurotransmitters

On account of the observed increase in SNARE complex assembly,

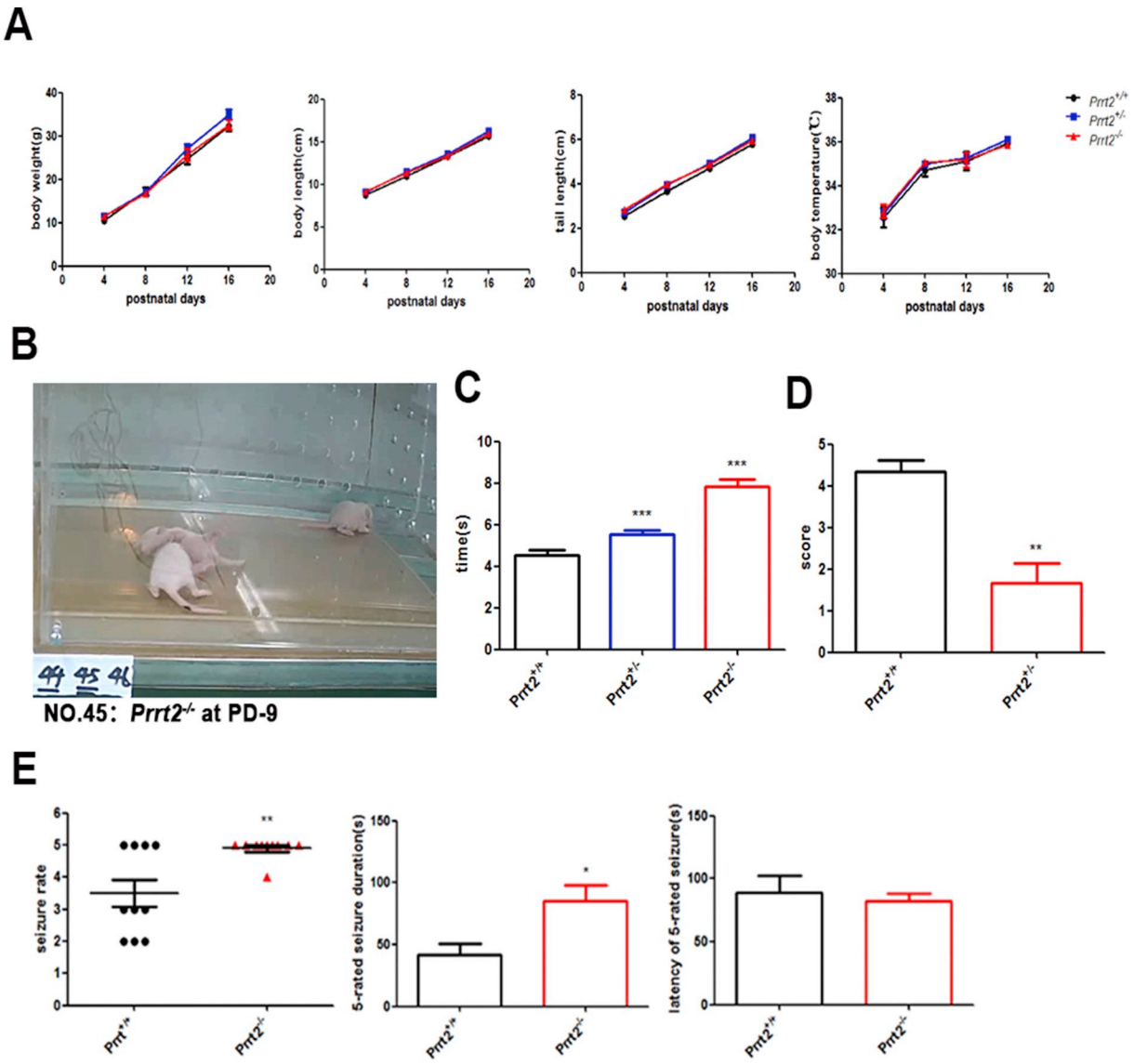

Fig. 3. *Prrt2*^{mut} rats showed apparent decline in motor coordination and poor tolerance to PTZ.

(A) Somatic growth indices including body weight, body length, tail length, and body temperature of both wild type and mutant rats at postnatal days 4, 8, 12, and 16 were tested; no significant difference was observed among the three genotypes. Error bars, mean ± SEM; $n = 8$ for both WT and *Prrt2*$^{-/-}$, $n = 16$ for *Prrt2*$^{+/-}$, two-way ANOVA.

(B) Involuntary PKC-like attacks were observed with low frequency in *Prrt2*$^{-/-}$ rats.

(C) *Prrt2*$^{-/-}$ rats required more time to go through the same beam in the beam balance test. Error bars, mean ± SEM; $n = 10$ littermates for WT, *Prrt2*$^{+/-}$, and *Prrt2*$^{-/-}$, $^{***}P < .001$ vs *Prrt2*$^{+/+}$, paired *t*-test.

(D) Coat hanger test results showed that *Prrt2*$^{-/-}$ rats had lower scores compared to wild type. Error bars, mean ± SEM; n = 10 littermates for WT and *Prrt2*$^{-/-}$ rats, $^{**}P < .01$ vs *Prrt2*$^{+/+}$, paired *t*-test.

(E) PTZ-induced seizure. After i.p. injection of PTZ (60 mg/kg), the seizure rate, latency, and 5-rated seizure duration of WT and *Prrt2*$^{-/-}$ rats were recorded. Error bars, mean ± SEM; n = 10 littermates for WT and *Prrt2*$^{-/-}$ rats, $^{*}P < .05$ and $^{**}P < .01$ vs *Prrt2*$^{+/+}$, unpaired *t*-test.

we visualized synaptic vesicles and measured content of amino acid neurotransmitters in the M1 cortex. Compared to *Prrt2*$^{+/+}$ rats, transmission electron microscopy (TEM) showed that in the M1 cortex of *Prrt2*$^{-/-}$ rats there were more vesicles docking in the active zones of the presynaptic membranes (+/+, 5.20 ± 0.34; −/−, 9.35 ± 0.37, $P < .0001$) (Fig. 5A and B). The M1 organic contents of aspartate (Asp) (+/+, 970.67 ± 249.53 ng/mg; −/−, 840.92 ± 107.63 ng/mg; $P = .4477$), glutamate (Glu) (+/+, 2370.98 ± 382.48 ng/mg; −/−, 2625.66 ± 303.00 ng/mg; $P = .3695$), glycine (Gly) (+/+, 75.14 ± 5.56 ng/mg; −/−, 84.48 ± 11.07 ng/mg; $P = .5297$) and γ-aminobutyric acid (GABA) (+/+, 334.42 ± 27.38 ng/mg; −/−, 351.95 ± 37.58 ng/mg; $P = .7177$), as detected by high performance liquid chromatography (HPLC)(Fig. 5D), did not differ between *Prrt2*$^{+/+}$ and *Prrt2*$^{-/-}$ rats (Supplementary Information, Fig. S2). However, as we collected the extracellular fluid of M1 neurons using microdialysis (Fig. 5C), we found that the concentrations of Asp (+/+, 332.48 ± 24.01 ng/mL; −/−, 734.27 ± 145.81 ng/mL; $P = .0362$), Glu (+/+, 4692.40 ± 1826.87 ng/mL; −/−, 9627.81 ± 3155.71 ng/mL; $P = .0474$), Gly (+/+, 1518.83 ± 325.21 ng/mL; −/−, 3572.13 ± 322.73 ng/mL; $P = .0224$), and GABA (+/+, 3265.25 ± 662.51 ng/mL; −/−, 6479.52 ± 851.97 ng/mL; $P = .0331$) were all significantly higher in *Prrt2*$^{-/-}$ rats (Fig. 5E), which indicated that the release of neurotransmitters was increased.

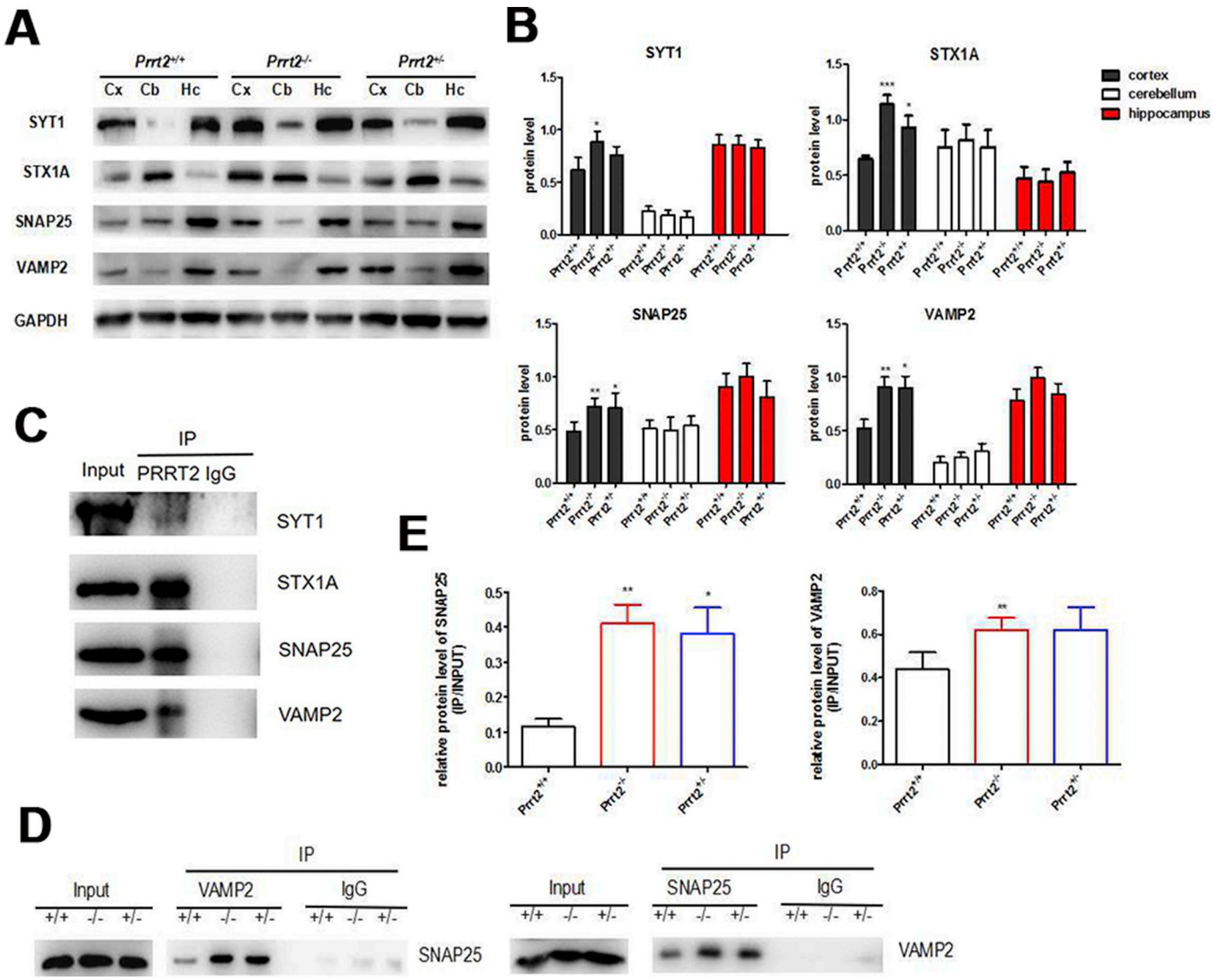

Fig. 4. PRRT2 negatively regulates SNARE complex formation in M1.
(A-B) Western blot showed that levels of SNAP25, STX1A, VAMP2, and SYT1 all rose significantly in the primary motor cortex (M1) of *Prrt2*$^{-/-}$ rats. (A) Representative immunoblots. GAPDH served as an internal control. (B) Quantification of Western blot results. Error bars, mean ± SEM; $n = 5–7$; *$P < .05$, **$P < .01$, and ***$P < .001$ vs *Prrt2*$^{+/+}$, paired *t*-test.
(C) Co-IP confirmed that PRRT2 interacted with SNAP25, STX1A, and VAMP2 in M1. IgG was used as a negative control.
(D-E) Co-IP verified that the interaction between SNAP25 and VAMP2 is significantly increased in M1 of *Prrt2*$^{-/-}$ rats. This result indicated that assembly of the SNARE complex is increased. (D) Representative immunoblots. IgG was used as a negative control. (E) Quantification of Western blot results. Error bars, mean ± SEM; n = 5–7; *$P < .05$ and **$P < .01$ vs *Prrt2*$^{+/+}$, paired *t*-test.

3.6. Imbalance between excitatory and inhibitory neuronal activity in the M1 cortex of Prrt2$^{-/-}$ *rat*

In addition to release of neurotransmitters, the levels of receptors embedded in the postsynaptic density are another parameter relevant to neuronal excitability. We verified the interaction between PRRT2 and GRIA1 in the M1 cortex of rat by co-IP (Fig. 6A) and measured protein levels of glutamate and glutamate receptors' important subunits GRIA1 and GABRA1. Compared to *Prrt2*$^{+/+}$ rats, the protein level of glutamate receptors in the M1 cortex of *Prrt2*$^{-/-}$ rats was significantly higher, while an opposite relationship was observed for glutamate receptors (Fig. 6B and C).

We further recorded electrophysiologic parameters of neurons in the M1 cortex of both *Prrt2*$^{+/+}$ and *Prrt2*$^{-/-}$ rats. In *Prrt2*$^{-/-}$ rats, mEPSC frequency (+/+, 12.06 ± 2.07; −/−, 18.63 ± 1.79, $P = .0228$) and amplitude (+/+, −14.26 ± 0.67; −/−, −19.88 ± 1.19, $P = .0003$) were significantly higher than *Prrt2*$^{+/+}$ rats (Fig. 6D and E), while mIPSC amplitude (+/+, 44.49 ± 3.34; −/−, 30.45 ± 4.29, $P = .02$) was significantly lower (Fig. 6Fand 6G) and the EPSC/IPSC ratio (+/+, 0.54 ± 0.03; −/−, 0.77 ± 0.03, $P = .0002$) was significantly higher (Fig. 6H). These findings demonstrate disruption of the balance between excitatory and inhibitory neuronal activity in the M1 cortex of *Prrt2*$^{-/-}$ rats, which could lead to abnormal neuronal hyperexcitability and ultimately cause PKC.

4. Discussion

Seizures in PKC patients are usually triggered by sudden voluntary movements. Clinical data from patients showed that PKC is associated with specific lesions of the motor loops (Hayashi et al., 1997; Volonté et al., 2001). The imbalance between increased excitatory projections and the impaired inhibitory projections within these loops is considered an underlying feature of movement disorders (Vitek, 2002; Hallett, 2006). Investigations of patients showed spontaneous brain

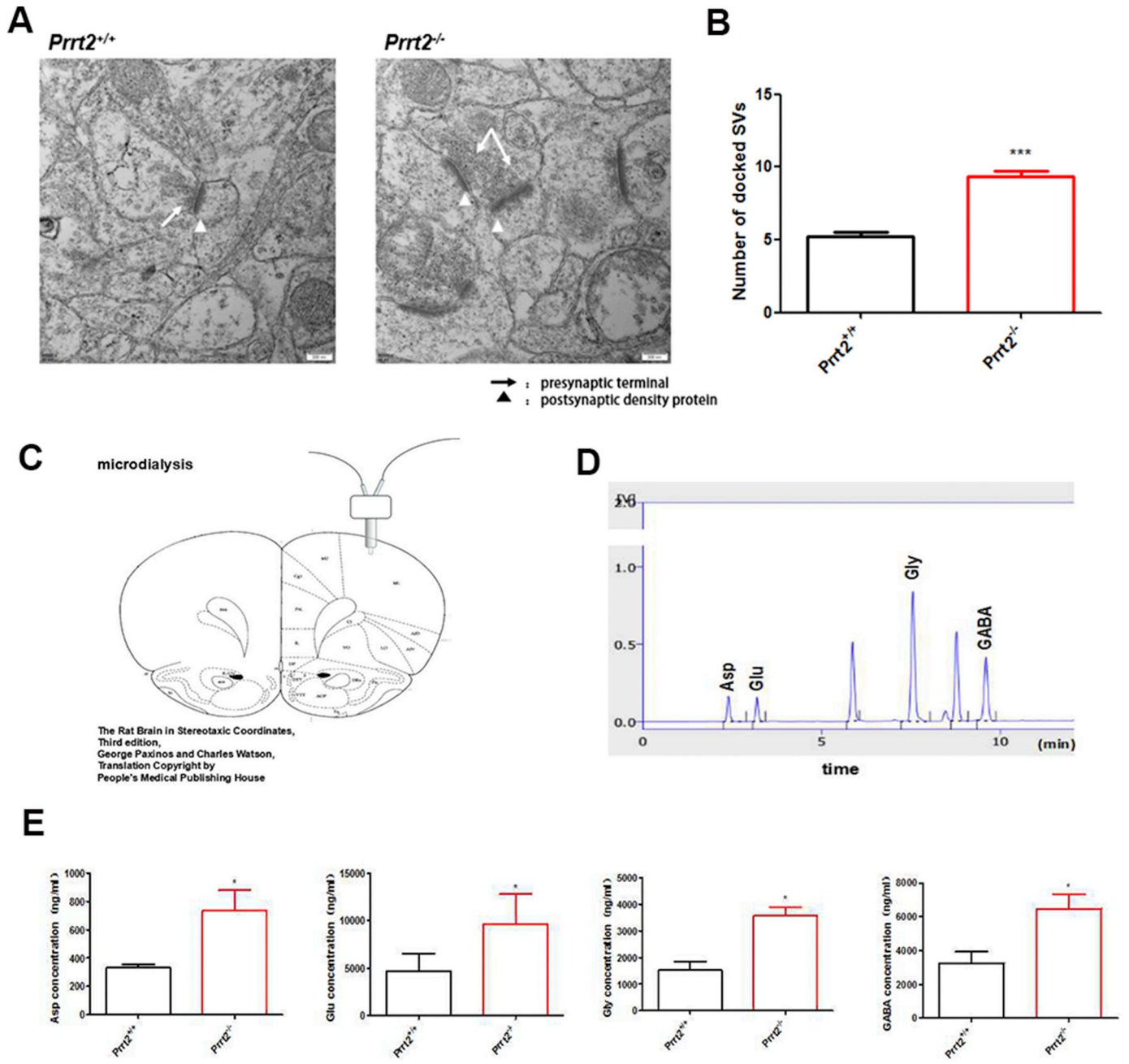

Fig. 5. Neurotransmitter release increased in M1 of *Prrt2*$^{-/-}$ rats.

(A-B) There were more vesicles docking in the active zones of the presynaptic membranes in M1 of P35 rats. (A) Representative TEM images. Scale bar, 200 nm. (B) Quantities of vesicles in TEM images. Error bars, mean ± SEM; $n = 30$ images of synapses for WT and mutant; *$P < .05$, **$P < .01$ and ***$P < .001$ vs *Prrt2*$^{+/+}$, unpaired *t*-test.

(C) Microdialysis experiment to collect the extracellular fluid of neurons in M1 of *Prrt2*$^{+/+}$ and *Prrt2*$^{-/-}$ rats.

(D) Representative HPLC chromatogram of amino acid mixture.

(E)HPLC results showed that the concentrations of Asp, Glu, Gly, and GABA released into the synaptic clefts were all significantly higher in M1 of *Prrt2*$^{-/-}$ rats compared to wild type littermates. Error bars, mean ± SEM; n = 5–6; *$P < .05$ vs *Prrt2*$^{+/+}$, paired *t*-test.

hyperactivity in the cortical-basal ganglia circuit, especially in the motor preparation and initiation areas (Zhou et al., 2010; Luo et al., 2013), and increased cerebral blood flow (CBF) in the motor cortex, basal ganglia, and thalamus (Ko et al., 2001; Shirane et al., 2001; Thiriaux et al., 2002). However, previous studies suggested that PKC was a disorder of the motor and premotor cortex (Franssen et al., 1983; Busard et al., 1984; Fattapposta et al., 2003). Among the components of motor loops, the primary motor cortex (M1) is a vital part and plays a central role in movement. Therefore, we hypothesized that abnormal physiological function of this area was related to PKC.

In this study, we generated *Prrt2* truncated mutant rats by CRISPR/Cas9-mediated genome editing. This rat model with some clinical features of PKC could contribute to researching the physiological function of PRRT2 and the pathogenesis of PKC. The subcellular location of PRRT2 has been controversial. Some studies on rat suggested that PRRT2 was present on both pre- and post-synaptic membranes (Liu et al., 2016), while others on mouse indicated that PRRT2 existed only on pre-synaptic membranes (Tan et al., 2018). Our results on rat corroborated that PRRT2 was specifically expressed in neurons, in both pre- and post-synaptic membranes. This was consistent with its

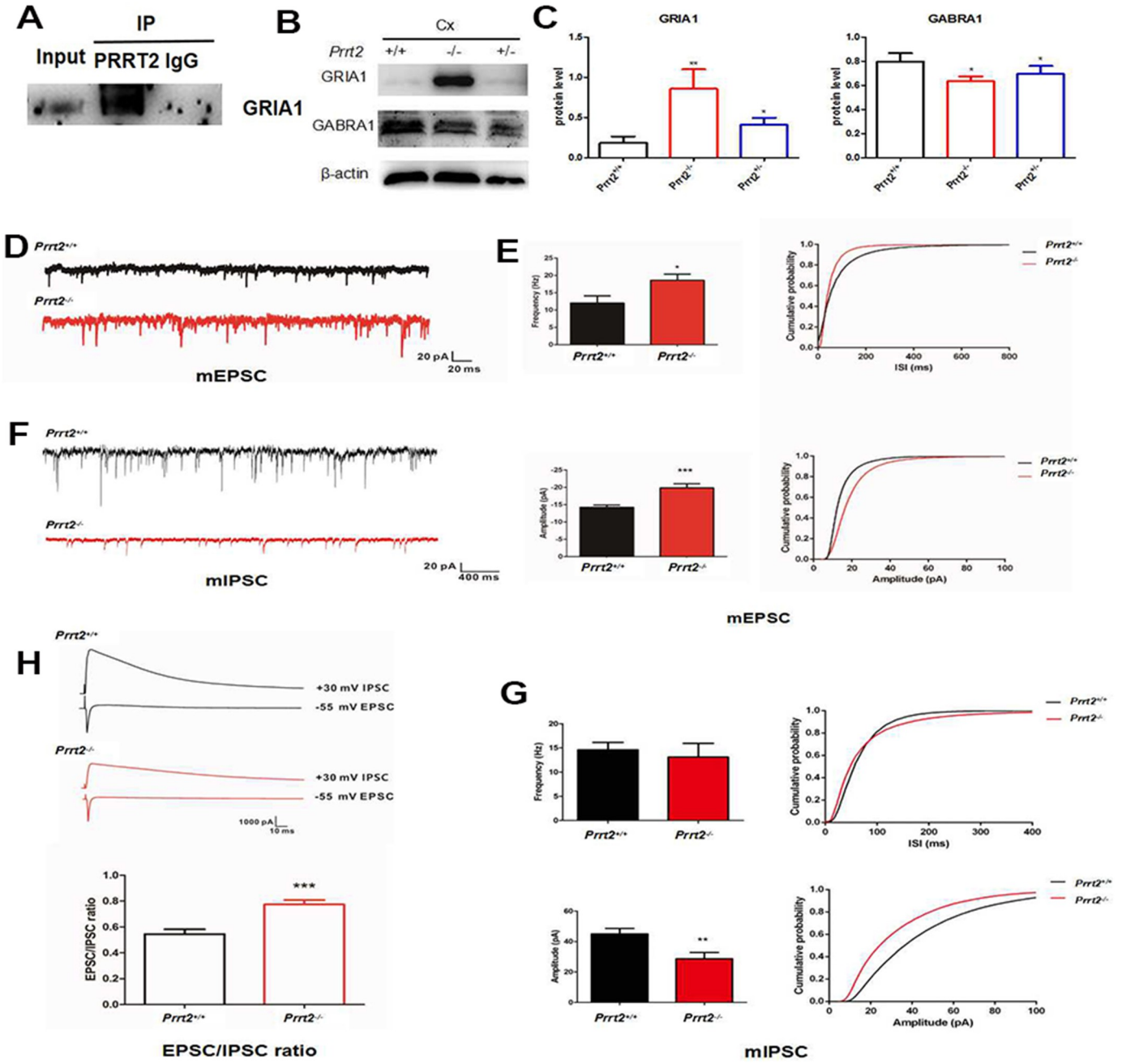

Fig. 6. Neuronal hyperexcitability in M1 of *Prrt2*$^{-/-}$ rats.
(A) Co-IP verified that PRRT2 interacted with GRIA1.
(B–C) Western blot showed that GRIA1 was significantly higher in M1 of *Prrt2*$^{-/-}$ rats compared to wild type littermates, while the opposite was observed for GABRA1 in M1. (B) Representative immunoblots. β-actin served as an internal control. (C) Quantification of Western blot results. Error bars, mean ± SEM; n = 7; *P < .05 and **P < .01 vs *Prrt2*$^{+/+}$, paired t-test.
(D-E) mEPSC frequency and amplitude were significantly higher in M1 of *Prrt2*$^{-/-}$ rats compared to wild type littermates. (D) Representative mEPSC recording in M1 slices of *Prrt2*$^{+/+}$ and *Prrt2*$^{-/-}$ rats. (E) Cumulative frequency and amplitude distribution curves of mEPSCs in M1 slices of *Prrt2*$^{+/+}$ and *Prrt2*$^{-/-}$ rats. Error bars, mean ± SEM; n = 16; *P < .05 and ***P < .001 vs *Prrt2*$^{+/+}$, unpaired t-test.
(F-G) The amplitude of mIPSC was significantly lower in M1 slices of *Prrt2*$^{-/-}$ rats compared to wild type littermates. (F) Representative recording of mIPSC in M1 slices of *Prrt2*$^{+/+}$ and *Prrt2*$^{-/-}$ rats. (G) Cumulative frequency and amplitude distribution curves of mIPSCs in M1 slices of *Prrt2*$^{+/+}$ and *Prrt2*$^{-/-}$ rats. Error bars, mean ± SEM; n = 10; **P < .01 vs *Prrt2*$^{+/+}$, unpaired *t*-test.
(H) The EPSC/IPSC ratio was significantly higher in M1 slices of *Prrt2*$^{-/-}$ rats compared to wild type littermates. Error bars, mean ± SEM; n = 10; ***P < .001 vs *Prrt2*$^{+/+}$, unpaired *t*-test.

interaction with SNAP25 (Stelzl et al., 2005) and GRIA1 (Schwenk et al., 2012).

It was reported that the N-terminal proline-rich region of PRRT2 could interact with SNAP25 and VAMP2. This interaction introduced steric hindrance that impeded the SNARE assembly (Coleman et al., 2018). Our study demonstratd that PRRT2 negatively regulates the process of vesicle release. The increase in synapse-associated proteins observed in *Prrt2*$^{-/-}$ rats may be a feedback of the up-regulating SNARE assembly.

Glutamate is the major excitatory neurotransmitter in the central

nervous system, while GABA is the major inhibitory neurotransmitter. However, the mechanisms mediating the change of glutamate and GABA receptor levels were unknown. We hypothesized that it was related to protein-protein interaction, but this remained to be demonstrated. Therefore, we proposed that the balance between excitatory and inhibitory neurons in the M1 cortex of *Prrt2*$^{-/-}$ rats is disrupted. We tested this directly by recording electrophysiologic parameters of M1 cortical neurons of both *Prrt2*$^{+/+}$ and *Prrt2*$^{-/-}$ rats. The results verified increased neuronal excitability in the M1 cortex of the rat model.

Other researchers had first reported that conditional knockout of *Prrt2* in cerebellar granule cells (GCs) of mouse was sufficient to induce dyskinesia attacks (Tan et al., 2018). Furthermore, there was a view that the occurrence of dystonia was a combinatorial effect of cortical-basal ganglia circuitry dysfunction and cerebellar circuitry dysfunction (Neychev et al., 2008). Clinical investigations indicated that the increased interhemispheric resting-state functional connectivity (RSFC) in PKC patients mainly occurred in the basal ganglia-thalamo-cortical circuitry and cerebellum (Ren et al., 2015). So, besides the M1 cortex, other regions including the basal ganglia may also play a role for the pathogenesis, which need to be explored further in our future research.

In conclusion, our research showed that PRRT2 could affect the release of amino acid neurotransmitters by regulating SNARE assembly on pre-synaptic membranes, interacting with GRIA1, and changing the protein levels of receptors on the post-synaptic membrane in the M1 cortex of rats. PRRT2 mutation lead to an imbalance between excitatory and inhibitory neuronal activity in the M1 cortex of *Prrt2*$^{-/-}$ rats. This neural hyperexcitability in M1 cortex is likely directly related to the PKC-like phenotype of *Prrt2*$^{-/-}$ rats. Thus, our findings are a meaningful extension of our previous studies and provide important insights into the physiological function of PRRT2 and the pathogenesis of PKC.

Supplementary data to this article can be found online at https://doi.org/10.1016/j.nbd.2018.10.011.

Acknowledgments

This work was supported by the National Natural Science Foundation of China [grant numbers 31371067, 31650004] and the Graduate Student Innovation Foundation of Peking Union Medical College [grant number 2016-0710-06].

Author contributions

Juan Mo and Bantong Wang designed the research, carried out the major experiments, analyzed the researched data, and wrote the manuscript.

Xilin Zhu designed the research, generated the animal model, analyzed the researched data, and contributed to experiments and discussion.

Xiaopan Wu contributed to discussion.

Ying Liu contributed to project design, management and researched data, wrote the manuscript.

All authors reviewed the manuscript.

Conflicts of interest

The authors declare no conflicts of interest.

References

Becker, F., Schubert, J., Striano, P., et al., 2013. PRRT2-related disorders: further PKD and ICCA cases and review of the literature. J. Neurol. 260 (5), 1234–1244.
Bhatia, K.P., 2011. Paroxysmal dyskinesias. Mov. Disord. 26, 1157–1165.
Bruno, M.K., Hallett, M., Gwinn-Hardy, K., et al., 2004. Clinical evaluation of idiopathic paroxysmal kinesigenic dyskinesia: new diagnostic criteria. Neurology 63, 2280–2287.
Busard, H.L., Renier, W.O., Gabreels, F.J., Vos, A.J., Declerck, A.C., Verhey, F.H., 1984. Autosomal dominant paroxysmal kinesigenic choreoathetosis. An electro-neurophysiological study. Clin Neurol Neurosurg 86, 281–289.
Cao, L., Huang, X.J., Zheng, L., et al., 2012. Identification of a novel PRRT2 mutation in patients with paroxysmal kinesigenic dyskinesias and c.649dupC as a mutation hot-spot. Parkinsonism Relat. Disord. 18 (5), 704–706.
Chen, W.J., Lin, Y., Xiong, Z.Q., et al., 2011. Exome sequencing identifies truncating PRRT2 that cause paroxysmal kinesigenic dyskinesia. Nat. Genet. 43 (12), 1252–1255.
Cohen, R.S., Blomberg, F., Berzins, K., et al., 1977. The structure of postsynaptic densities isolated from dog cerebral cortex. I. Overall morphology and protein composition. J Cell Biol. 74 (1), 181–203.
Coleman, J., Jouannot, O., Ramakrishnan, S.K., et al., 2018. PRRT2 regulates synaptic fusion by directly modulating SNARE complex assembly. Cell Rep. 22 (3), 820–831.
Demirkiran, M., Jankovic, J., 1995. Paroxysmal dyskinesias: clinical features and classification. Ann. Neurol. 38, 571–579.
Du, T., Feng, B., Wang, X., et al., 2008. Localization and mutation detection for kinesigenic choreoathetosis. J. Mol. Neurosci. 34 (2), 101–107.
Ebrahimi-Fakhari, D., Saffari, A., Westenberger, A., et al., 2015. The evolving spectrum of PRRT2-associated paroxysmal diseases. Brain 138, 3476–3495.
Fattapposta, F., My, F., Valente, D., et al., 2003. Preprogramming motor dysfunction in paroxysmal kinesigenic choreoathetosis. Funct. Neurol. 18, 29–34.
Franssen, H., Fortgens, C., Wattendorff, A.R., van Woerkom, T.C., 1983. Paroxysmal kinesigenic choreoathetosis and abnormal contingent negative variation. A case report. Arch. Neurol. 40, 381–385.
Fruscione, F., Valente, P., Sterlini, B., et al., 2018. PRRT2 controls neuronal excitability by negatively modulating Na^+ channel 1.2/1.6 activity. Brain 141 (4), 1000–1016 Apr 1.
Goodenough, D.J., Fariello, R.G., Annis, B.L., et al., 1978. Familial and acquired paroxysmal dyskinesias. A proposed classification with delineation of clinical features. Arch. Neurol. 35, 827–831.
Ha, Tomita, Nagamitsu, S., Wakui, K., et al., 1999. Paroxysmal kinesigenic choreoathetosis maps to chromosome 16p11.2-q12.1. Am. J. Hum. Genet. 65 (6), 1688–1697.
Hallett, M., 2006. Pathophysiology of dystonia. J. Neural Transm. Suppl. 70, 485–488.
Hayashi, R., Hanyu, N., Yahikozawa, H., et al., 1997. Ictal muscle discharge pattern and SPECT in paroxysmal kinesigenic choreoathetosis. Electromyogr. Clin. Neurophysiol. 37, 89–94.
Heron, S.E., Grinton, B.E., Kivity, S., et al., 2012. PRRT2 mutations cause benign familial infantile epilepsy and infantile convulsions with choreoathetosis syndrome. Am. J. Hum. Genet. 90 (1), 152–160.
Jahn, R., Fasshauer, D., 2012. Molecular machines governing exocytosis of synaptic vesicles. Nature 490 (7419), 201–207.
Kertesz, A., 1967. Paroxysmal kinesigenic choreoathetosis. An entity within the paroxysmal choreoathetosis syndrome. Description of 10 cases, including 1 autopsied. Neurology 17, 680–690.
Klein, C., Vieregge, P., 1998. Non-epileptic paroxysmal movement disorders. Nervenarzt 69, 647–659.
Ko, C.H., Kong, C.K., Ngai, W.T., et al., 2001. Ictal (99m)Tc ECD SPECT in paroxysmal kinesigenic choreoathetosis. Pediatr. Neurol. 24 (3), 225–227.
Lee, H.Y., Huang, Y., Bruneau, N., et al., 2012. Mutations in the gene PRRT2 cause paroxysmal kinesigenic dyskinesia with infantile convulsions. Cell Rep. 1 (1), 2–12.
Li, J., Zhu, X., Wang, X., et al., 2012. Targeted genomic sequencing identifies PRRT2 mutations paroxysmal kinesigenic choreoathetosis. J. Med. Genet. 49, 76–78.
Li, M., Niu, F., Zhu, X., et al., 2015. PRRT2 mutant leads to dysfunction of glutamate signaling. Int. J. Mol. Sci. 16, 9134–9151.
Liu, Q., Qi, Z., Wan, X.H., et al., 2012. Mutations in PRRT2 result in paroxysmal dyskinesias marked variability in clinical expression. J. Med. Genet. 49 (2), 79–82.
Liu, Y.T., Nian, F.S., Chou, W.J., et al., 2016. PRRT2 mutations lead to neuronal dysfunction and neurodevelopmental defects. Oncotarget 7 (26), 39184–39196.
Long, Z., Xu, Q., Miao, H.H., et al., 2017. Thalamocortical dysconnectivity in paroxysmal kinesigenic dyskinesia: Combining functional magnetic resonance imaging and diffusion tensor imaging. Mov. Disord. 32, 592–600.
Luo, C., Chen, Y., Song, W., et al., 2013. Altered intrinsic brain activity in patients with paroxysmal kinesigenic dyskinesia by PRRT2 mutation: altered brain activity by PRRT2 mutation. Neurol. Sci. 34 (11), 1925–1931.
Marini, C., Conti, V., Mei, D., et al., 2012. PRRT2 mutations in familial infantile seizures, paroxysmal dyskinesia, and hemiplegic migraine. Neurology 79, 2109–2114.
Méneret, A., Gaudebout, C., Riant, F., et al., 2013. PRRT2 mutations and paroxysmal disorders. Eur. J. Neurol. 20 (6), 872–878.
Michetti, C., Corradi, A., Benfenati, F., 2017. PRRT2, a network stability gene. Oncotarget 8 (34), 55770–55771 Jul 24.
Neychev, V.K., Fan, X., Mitev, V.I., et al., 2008. The basal ganglia and cerebellum interact in the expression of dystonic movement. Brain 131 (9), 2499–2509. https://doi.org/10.1093/brain/awn168. (Epub 2008 Jul 26).
Okumura, A., Shimojima, K., Kubota, T., et al., 2013. PRRT2 mutation in Japanese children with benign infantile epilepsy. Brain and Development 3, 641–646.
Ono, S., Yoshiura, K., Kinoshita, A., et al., 2012. Mutations in PRRT2 responsible for paroxysmal kinesigenic dyskinesias also cause benign familial infantile convulsions. J. Hum. Genet. 57 (5), 338–341.
Paxinos, George, Watson, Charles, 2007. The Rat Brain in Stereotaxic Coordinates. Third Edition Burlington USA.
Racine, R.J., 1972. Modification of seizure activity by electrical stimulation. II. Motor seizure. Electroencephalogr Clin Neurophysiol. 32 (3), 281–294.
Ren, J., Lei, D., Yang, T., et al., 2015. Increased interhemispheric resting-state functional connectivity in paroxysmal kinesigenic dyskinesia: a resting-state fMRI study. J. Neurol. Sci. 351, 93–98.

Rossi, P., Sterlini, B., Castroflorio, E., et al., 2016. Novel topology of proline-rich transmembrane protein 2 (PRRT2): hints for an intracellular function at the synapse. J. Biol. Chem. 291 (12), 6111–6123. https://doi.org/10.1074/jbc.M115.683888. (Epub 2016 Jan 21).
Schmidt, A., Kumar, K.R., Redyk, K., et al., 2012. Two faces of the same coin: benign familial infantile seizures and paroxysmal kinesigenic dyskinesia caused by PRRT2 mutations. Arch. Neurol. 69, 668–670.
Schubert, J., Paravidino, R., Becker, F., et al., 2012. PRRT2 mutations are the major cause of benign familial infantile seizures. Hum. Mutat. 33, 1439–1443.
Schwenk, J., Harmel, N., Brechet, A., et al., 2012. High-resolution proteomics unravel architecture and molecular diversity of native AMPA receptor complexes. Neuron 74 (4), 621–633.
Shirane, S., Sasaki, M., Kogure, D., et al., 2001. Increased ictal perfusion of the thalamus in paroxysmal kinesigenic dyskinesia. J. Neurol. Neurosurg. Psychiatry 71, 408–410.
Stelzl, U., Worm, U., Lalowski, M., et al., 2005. A human protein-protein interaction network: a resource for annotating the proteome. Cell 122 (6), 957–968.
Tan, G.H., Liu, Y.Y., Wang, L., et al., 2018. PRRT2 deficiency induces paroxysmal kinesigenic dyskinesia by regulating synaptic transmission in cerebellum. Cell Res. 28 (1), 90–110.
Thiriaux, A., de St Martin, A., Vercueil, L., et al., 2002. Co-occurrence of infantile epileptic seizures and childhood paroxysmal choreoathetosis in one family: clinical, EEG, and SPECT characterization of episodic events. Mov. Disord. 17 (1), 98–104.
Valente, P., Castroflorio, E., Rossi, P., et al., 2016. PRRT2 is a key component of the Ca2 + − dependent neurotransmitter release machinery. Cell Rep. 15 (1), 117–131.
Valtorta, F., Benfenati, F., Zara, F., et al., 2016. PRRT2: from paroxysmal disorders to regulation of synaptic function. Trends Neurosci. 39 (10), 668–679.
Vitek, J.L., 2002. Pathophysiology of dystonia: a neuronal model. Mov. Disord. 17 (Suppl. 3), S49–S62.
Volonté, M.A., Perani, D., Lanzi, R., et al., 2001. Regression of ventral striatum hypometabolism after calcium/calcitriol therapy in paroxysmal kinesigenic choreoathetosis due to idiopathic primary hypoparathyrodism. J. Neurol. Neurosurg. Psychiatry 71, 691–695.
Wang, X., Sun, W., Zhu, X., et al., 2010. Paroxysmal kinesigenic choreoathetosis: evidence to the pericentromeric region of chromosome 16 in four Chinese families. Eur. J. Neurol. 17 (6), 800–807.
Wang, J.L., Cao, L., Li, X.H., et al., 2011. Identification of PRRT2 as the causative paroxysmal kinesigenic dyskinesias. Brain 134 (Pt 12), 3493–3501.
Yang, Y., Xia, Z., Liu, Y., 2000. SNAP-25 functional domains in SNARE core complex assembly and glutamate release of cerebellar granule cells. J. Biol. Chem. 275, 29482–29487.
Zhou, B., Chen, Q., Zhang, Q., et al., 2010. Hyperactive putamen in patients with paroxysmal kinesigenic choreoathetosis: a resting-state functional magnetic resonance imaging study. Mov. Disord. 25, 1226–1231.